Structural Engineering and Mechanics, *Vol. 69, No. 6 (2019) 627-635*
DOI: https://doi.org/10.12989/sem.2019.69.6.627

Mechanical performance of sand-lightweight concrete-filled steel tube stub column under axial compression

Xianggang Zhang*[1,2], Dapeng Deng[2], Xinyan Lin[1,2], Jianhui Yang[1,2] and Lei Fu[1,2]

[1]*Henan Province Engineering Laboratory of Eco-Architecture and the Built Environment, Henan Polytechnic University, Jiaozuo, Henan, China*
[2]*School of Civil Engineering, Henan Polytechnic University, Jiaozuo, Henan, China*

(Received June 21, 2018, Revised January 26, 2019, Accepted January 30, 2019)

Abstract. In order to study the axial compression performance of sand-lightweight concrete-filled steel tube (SLCFST) stub columns, three circular SLCFST (C-SLCFST) stub column specimens and three SLCFST square (S-SLCFST) stub column specimens were fabricated and static monotonic axial compression performance testing was carried out, using the volume ratio between river sand and ceramic sand in sand-lightweight concrete (SLC) as a varying parameter. The stress process and failure mode of the specimens were observed, stress-strain curves were obtained and analysed for the specimens, and the ultimate bearing capacity of SLCFST stub column specimens was calculated based on unified strength theory, limit equilibrium theory and superposition theory. The results show that the outer steel tubes of SLCFST stub columns buckled outward, core SLC was crushed, and the damage to the upper parts of the S-SLCFST stub columns was more serious than for C-SLCFST stub columns. Three stages can be identified in the stress-strain curves of SLCFST stub columns: an elastic stage, an elastic-plastic stage and a plastic stage. It is suggested that AIJ-1997, CECS 159:2004 or AIJ-1997, based on superposition theory, can be used to design the ultimate bearing capacity under axial compression for C-SLCFST and S-SLCFST stub columns; for varying replacement ratios of natural river sand, the calculated stress-strain curves for SLCFST stub columns under axial compression show good fitting to the test measure curves.

Keywords: sand-lightweight concrete-filled steel tube; stub column; cross section form; replacement ratio; ultimate bearing capacity under axial compression; complete curve between stress and strain

1. Introduction

As a type of lightweight aggregate concrete, all lightweight concrete has advantages including light (Shafigh *et al*. 2013), heat preservation and sound insulation (Tang 2017), good working performance (Chien *et al*. 2014) and excellent seismic performance (Carrillo *et al*. 2015); of these benefits, its low apparent density is the most prominent. This is very important in the application and popularisation of all lightweight concrete in high-rise buildings, space structures and large volume structures (Zhang *et al*. 2018). However, since coarse and fine lightweight aggregates are used for lightweight aggregate concrete, lightweight aggregate floatation is a serious problem (Obaidat and Haddad 2016). The strength of lightweight aggregate is very low, and it is therefore difficult for all lightweight concrete to meet design requirements (Ayati *et al*. 2018).

Using all lightweight concrete as a basis, a new type of lightweight aggregate concrete called SLC is made using natural river sand as a partial or complete substitute for lightweight sand in all lightweight concrete (Zhang *et al*. 2017). Compared with all lightweight concrete, SLC has a higher strength and elastic modulus (Yang and Ashour 2011), lower shrinkage deformation (Choi *et al*. 2014), and can reduce pumping and construction difficulties (Dong *et al*. 2016, Meng and Khayat 2017), greatly reducing the project costs (Amel *et al*. 2017).

Concrete-filled steel tubes are widely used in industrial and civil buildings due to their high bearing capacity, good plasticity and toughness, convenient methods of construction and good seismic performance (Min *et al*. 2013, Tao *et al*. 2016). Montejo *et al.* (2012), Zhang et al. (2015), Tu *et al.* (2014) and Liu *et al.* (2014) have extensively studied and reported on the static, long-term mechanical and hysteretic properties and fire resistance of concrete-filled steel tubes. SLCFST is formed by placing SLC inside a steel tube; this can not only offer the advantages of high strength, good plasticity and toughness, convenient construction methods and good seismic performance of concrete-filled steel tubes, but can also greatly improve the mechanical properties of core SLC through the confining pressure of the external steel pipes. SLCFST can reduce the self-weight of the concrete-filled steel tube and achieve the purpose of strengthening the constraint on the core material, and also protects the SLC from external harmful media erosion and deterioration. These factors mean that SLCFST can be adapted to the needs of modern engineering structures, which involve large spans, heavy loads and very high structures (Abdelgadir *et al*. 2011, Ghannam *et al*. 2004).

∗Corresponding author, Lecturer
E-mail: xgzhang1986@163.com

http://www.techno-press.com/journals/sem&subpage=7
ISSN: 1225-4568 (Print), 1598-6217 (Online)

At present, only a limited amount of research has been carried out on all lightweight concrete-filled steel tubes. Fu *et al.* (2016, 2014) studied the compressive and bending properties of all lightweight concrete-filled steel tubes, and the results showed that with an increase in the ratio of the steel area, the restraining effect of the steel tube on the lightweight aggregate concrete is increased; the moment capacity of all lightweight concrete-filled steel tubes increased as the steel ratio and core lightweight concrete strength increased. Assi *et al.* (2003) studied the contribution of lightweight aggregate and foamed concrete to the ultimate strength capacity of square and rectangular steel tube sections, finding that these materials can be used in composite constructions to increase the flexural capacity of steel tubular sections. AL-Eliwi *et al.* (2017) studied the performance of lightweight aggregate and self-compacted concrete-filled steel tube columns, and the results showed that the nature of the utilized lightweight aggregate led to the local buckling mode being dominant in lightweight concrete-filled steel tube columns. In all, these results show that the strength, modulus and plasticity of the core lightweight concrete are improved to varying degrees under the constraints of the external steel tube, and the stiffness of all-lightweight concrete-filled circular steel tube also improves. However, little research into SLCFST has been done.

On the basis of the above studies, C-SLCFST and S-SLCFST stub columns were designed and made in this study using shale ceramsite and shale pottery as lightweight aggregate with different replacement ratios of river sand. An axial compression performance test was carried out on the SLCFST stub columns to reveal the stress mechanism and failure mode, and the ultimate bearing capacity for axial compressive stress. The whole process of mechanical response was carefully analysed, and can provide a reference for further research and applications of SLCFST.

2. Overview of testing

2.1 Design and manufacture of specimens

Six SLCFST stub columns were designed, with two changing parameters: the cross-sectional form and the river sand replacement ratio. The cross-sectional forms of the steel tube were circular and square; three circular steel tubes and three square steel tubes were made, all of which were welded using a straight weld. The diameter of the round steel tube was 159 mm, while the length of the side of the steel tube was 150 mm. The river sand replacement ratio refers to the loose volume proportion of river sand in all fine aggregate. Its levels in this study were 0%, 50%, and 100%.

The raw material for the SLC was P, O 42.5R cement, fly ash, a water reducing agent, running water, natural river sand, shale ceramsite and shale pottery. The mixes of sand light concrete with three different replacement ratios are shown in Table 1. The sand light concrete with a strength grade of LC35 was made up based on a replacement ratio of 0%; the other types of replacement sand light concrete were made up by changing the loose volume ratio of the sand.

Table 1 Mix of sand-lightweight aggregate concrete (kg/m^3)

River sand replacement	Water	Cement	Fly ash	Water reducing agent	Shale ceramsite	Shale pottery	Natural river sand
0%	171	472	159	6.31	444	408	0
50%	171	472	159	6.31	444	204	341
100%	171	472	159	6.31	444	0	682

Table 2 Design parameters for specimens

No.	r	L	D	t	L/D	D/t	α	f_y	f_u	E	v	ε_y	f_{cu}	f_c	ξ
C-0	0%	480	159	3.5	3.02	45.43	0.0942	337	417	178	1.89	1891	35.8	24.7	1.29
C-1	50%	480	159	3.5	3.02	45.43	0.0942	337	417	178	1.89	1891	42.1	35.9	0.88
C-2	100%	480	159	3.5	3.02	45.43	0.0942	337	417	178	1.89	1891	44.8	42.4	0.75
S-0	0%	450	150	3.0	3.00	50.00	0.0851	268	342	161	1.67	1666	35.8	24.7	0.92
S-1	50%	450	150	3.0	3.00	50.00	0.0851	268	342	161	1.67	1666	42.1	35.9	0.64
S-2	100%	450	150	3.0	3.00	50.00	0.0851	268	342	161	1.67	1666	44.8	42.4	0.54

Note: r is the river sand replacement ratio; L is the height of the specimen (mm); D is the outer diameter of the circular steel tube or the outer side length of the square steel tube (mm); t is the thickness of the steel tube (mm); α is the steel ratio ($\alpha = A_s/A_c$, A_s, A_c stand for the cross-sectional area of the steel tube and SLC, respectively); f_y, f_u are the yield strength and ultimate strength of the steel tube (MPa), respectively; E is the modulus elasticity of the steel tube (GPa); v is the Poisson's ratio for the steel tube; ε_y is the yield strain of the steel tube; f_{cu}, f_c are the cube compressive strength and axial compressive strength of the SLC corresponding to the specimens (MPa); and ξ is the hoop coefficient (for $\alpha f_y/f_c$).

Second level fly ash was used, accounting for 25% of the total cement material, and the main ingredient of the water-reducing agent was a β-high condensation compound of naphthalene sulphonic acid formaldehyde, in a mixing quantity of 1% of the total cementing material.

An 8 mm-thick end plate was welded at one end of the steel tube after it was made. The SLC was poured from the other end, and cube and prism standard test blocks were prepared in the same condition. After the specimens were completely cured, the same proportionate cement mortar was used to make the surface level, and another 8 mm-thick end plate was welded onto the tube so that the SLC was completely enclosed inside the steel tube. The design parameters for the specimens are shown in Table 2.

2.2 Test method

The test was carried out on a 500 t hydraulic press, and the loading device used is shown in Fig. 1. Load control was used in the test loading system, whereby each level of load was taken as $P_u/10$ (where P_u is the estimated ultimate load), and held for two minutes; when loaded to 0.90 P_u, it was transferred to displacement control, and the control displacement amplitude was about 3 mm, when strengthening sections appeared and developed on the loading-displacement curves till displacement reached to the maximal range of dial indicator, the test was ended. The axial strain and hoop strain of the external steel tube were

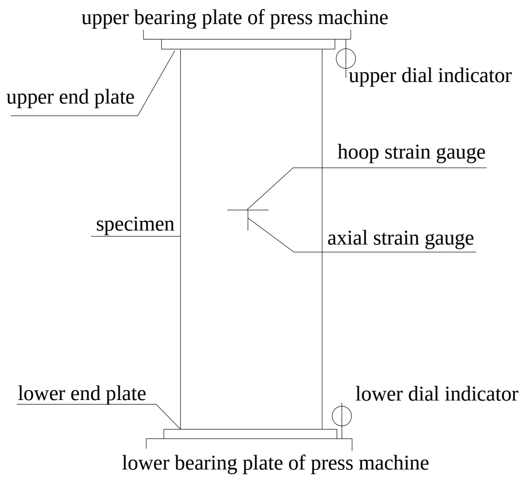

Fig. 1 Loading and measuring device used in testing

automatically recorded by the static strain collector, and displacement data and load values were acquired by the dial indicator and computer, respectively, as shown in Fig. 1.

3. Analysis and discussion of test results

3.1 Failure process and modes

In the initial stage of loading, there was no apparent change in the appearance of the specimens. When the load was increased to about 60% of the limit load, the core SLC began to emit the sound of fine colloid cracking, and when the load was increased to about 80%-90% of the limit load, the laitance and rust on the steel tube surface began to fall off, accompanied by a crackling sound, and the surface of the steel tube began to buckle. When the limit load was reached, the first buckling ring on the upper part of the steel tube had been formed. With the continuation of the load, the surface of the steel tube formed the second and third buckling in turn, and the intense splitting sound of lightweight aggregate was emitted from the specimen. Finally, the specimen was completely destroyed by the excessive deformation of the steel tube.

After the test, the external steel tube was opened and the failure mode of the core SLC was observed. The failure modes of the SLCFST stub column is shown in Fig. 2. As shown in Fig. 2(a) and (b), the outside of the circle and square steel tube were outwardly buckled. The buckling parts of the circular specimens were mainly concentrated in the upper, lower, and middle sections, and buckling parts of square specimens mainly concentrated in the upper regions. The buckling of the square steel tube was more serious; the individual square specimen appeared to be torn in the upper region of the pipe, and the steel pipe in the upper parts of some square specimens was torn. As shown in Fig. 2(c), the core SLC exhibited cracked and crushed areas along the whole height range of the round specimen, and there were signs of sliding-reshaping downward due to compression, with powdered SLC in the fracture section; in the half-height range for the square specimen, the core SLC was crushed, and the damage was more serious, while in the

(a) Circular steel tube

(b) Square steel tube

(c) Core SLC

Fig. 2 Failure modes for specimens

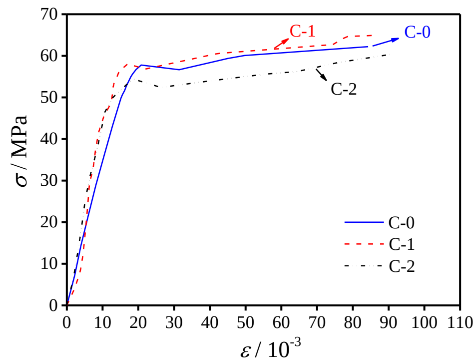

(a) Circular specimens

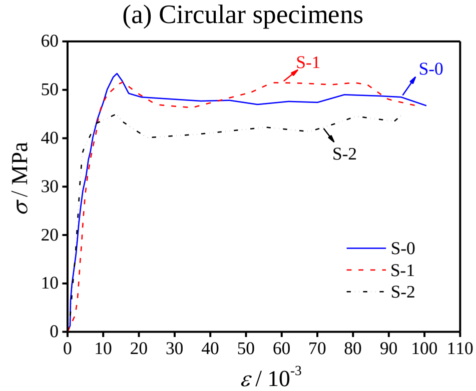

(b) Square specimens

Fig. 3 Measured stress-strain curves for specimens

Table 3 Degraded amplitudes and recovery amplitudes of axial bearing capacities for specimens

No.	C-0	C-1	C-2	S-0	S-1	S-2
First peak stress/MPa	57.78	58.08	54.44	53.36	51.78	45.02
Valley stress/MPa	56.65	56.8	52.40	46.97	46.31	40.10
Rising peak stress/MPa	62.21	64.90	60.35	48.99	51.47	44.93
Axial compression bearing capacity degenerate range	98.0%	97.8%	96.3%	88.0%	89.4%	89.1%
Axial compression bearing capacity recovery range	107.7%	111.7%	110.9%	91.8%	99.4%	99.8%

lower part of the core SLC, there was no evidence of cracking or crushing.

3.2 Measured stress-strain curves

The measured load and displacement for the SLCFST stub column were converted to nominal stress-strain curves using Eq. (1), as shown in Fig. 3

$$\sigma = N/A, \quad \varepsilon = \Delta l/l \tag{1}$$

where N is the axial compressive force of the specimen; A is the total cross-sectional area of the specimen; Δl is the compression displacement of the specimen during the stress process; and l is the specimen height.

As shown in Fig. 3, the nominal stress-strain curves for all SLCFST stub column specimens could be divided into three stages: a linear rise, slow growth and a slow drop/steady development. From the point of view of force performance, this phenomenon reflects the three loading stages (elastic, elastic-plastic and plastic) for the SLCFST stub column. In the elastic stage, the stress-strain curve for the SLCFST stub column is almost straight, and the elastic proportional limit load is about 50%-70% of the limit load. When the specimen enters the elastic-plastic stage, the outer circle and square steel tube gradually yielded, and the micro cracks in the core SLC continued to expand, leading to a significant increase in the longitudinal displacement of the specimen. the nominal stress-strain curve then gradually deviated from a straight line until it reached the peak point. At this point, the bearing capacity of the specimen reached the ultimate bearing capacity. When the specimen entered the plastic stage, the nominal stress-strain curve of the specimen showed a relatively gentle descent section; at this point, the yielding of the steel was more severe, and the vertical load was mainly borne by the core SLC. Compared with the square specimen, the binding distribution of the circular specimen's outer steel tube to the core SLC was more uniform; this is due to the effect of the external steel tube on the core SLC, whereby the hoop coefficient is high, the nominal stress-strain curve of the plastic stage slowly rises, and the bearing capacity of the specimen is larger than the ultimate bearing capacity at the end of the test. In the plastic stage of the nominal stress-strain curve for the square specimen, there are small fluctuations in the upper and lower stages, but the bearing capacity at the peak is less than the ultimate bearing capacity.

3.3 Degradation and recovery of axial compression bearing capacity

To define the axial compression bearing capacity degenerate range of the SLCFST stub columns, the ratio between the valley stress and peak stress in the measured stress-strain curve is used; to define the axial compression bearing capacity recovery range of the SLCFST stub column, the ratio of the rising peak stress to the first peak stress is used, where the maximum stress after the first peak stress is taken as the rising peak stress. The degradation and recovery range of the axial compression bearing capacity of the circular and square specimens are shown in Table 3. The stress-strain curve for the circular specimen shows a slow rise after reaching the valley, and the recovery peak stress is taken as the axial compression bearing stress at the end of loading.

As shown in Table 3, for circular specimens, the degradation and recovery range of the axial compression bearing capacity undergo very little change, and thus the river sand replacement ratio has little influence on the degradation and recovery range. The mean value of the degradation range for the axial compression bearing capacity is 97.37%, and the mean value of the recovery range for the axial compression bearing capacity is 110.10%. C-SLCFST stub columns can still maintain a high bearing capacity after reaching the ultimate load, and they show strengthening features. For the square specimens, the ratio of river sand replacement has little effect on the degradation and recovery range axial compression bearing capacity; the mean value of the degradation range of the axial compression bearing capacity is 88.83%, while the mean value of the recovery range for the axial compression bearing capacity is 97.00%. After it reaches the limit load, the axial compression bearing capacity of the upper part of the square steel tube and the SLC is greatly reduced, and its axial compression bearing capacity is greatly reduced. With continued loading, the yield range of the square steel tube increases, and the buckling hoop gradually becomes circular rather than square. The confining mechanism of the square steel tube on the SLC is close to that of the circular steel tube, and the steel itself is fully strengthened, so the axial compressive bearing capacity of square specimens also increases, although its recovery range is smaller than that of the circular specimen.

3.4 Load-axial strain curve for the steel tube

The axial strain of the external steel tube in the loading process can be measured using the axial strain gauge located in the central part of the external steel tube. The axial load(N)-axial strain(ε_a) of the C-SLCFST and S-SLCFST stub columns is shown in Fig. 4.

As shown in Fig. 4(a), in the initial stage of loading, the N-ε_a curve of the circular specimen rose linearly; when the turning point was reached, the specimen yielded due to axial compression, and the measured axial strain of the steel tube was fairly similar to that of the yield strain. After that, since the core SLC still had some bearing capacity under

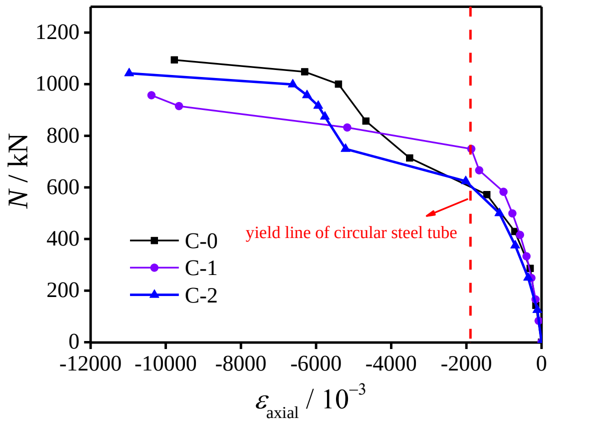

(a) Circular specimens

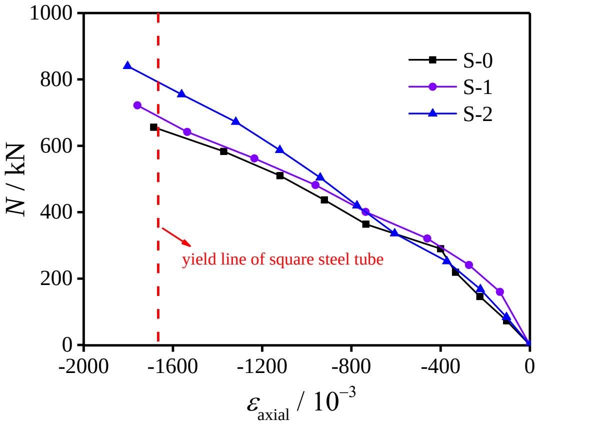

(b) Square specimens

Fig. 4 Relationships of column axial load-steel tube axial strain

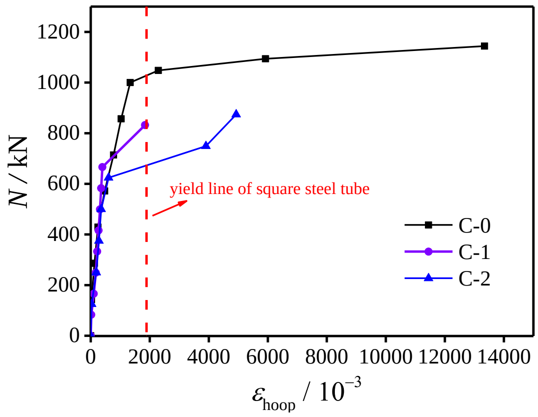

(a) Circular specimens

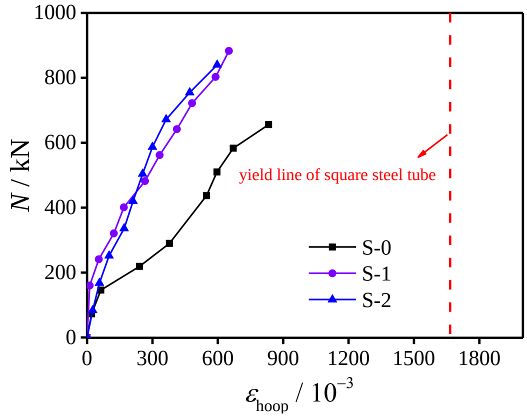

(b) Square specimens

Fig. 5 Relationships of column axial load-steel tube hoop strain

the constraint of the external circular steel tube, the N-ε_a curve rose slowly. Compared with the load, the strain of the steel tube increased rapidly, and the N-ε_a curve showed a long period of plastic deformation. Before the axial strain gauge was invalid, the axial compression strain measured for external steel tube of the circular specimen was more than 10,000 $\mu\varepsilon$, and the performance of the axial compression material of the external circular steel tube was fully developed. As shown in Fig. 4(b), similarly to the initial loading of the circular specimen, the axial compression strain of the square specimen increased approximately linearly with the increase in the load. When the load reached 70%-80% of the limit load, the axial deformation of the square specimen was too large and the axial strain gauge was damaged, and was unable to collect subsequent strain data; however, the data collected before failure exceeded the yield strain of the square steel tube. This also indicates that the axial deformation resistance of the square specimen was weaker than that of the circular specimen, and the overall performance of the external square steel tube and core SLC was relatively poor.

3.5 Load-hoop strain curve of the steel tube

The hoop strain of the external steel tube during the process of axial compression was collected using the hoop strain gauge positioned in the central part of the external steel tube, and the axial load (N)-hoop strain (ε_h) curves for the SLCFST stub columns are shown in Fig. 5.

As shown in Fig. 5, in the initial stage of loading, the hoop strain of the circular and square specimens increased linearly with an increase in the load, and was less than the axial compression strain. At this point, the external steel pipe was not involved in the core SLC constraints, as it was bearing the axial compression rather than the hoop tension. When the N-ε_h relation curve underwent a turning point, the specimen entered the axial compression yield state; at this stage, there was little difference between the hoop tensile strain and the yield strain of the steel pipe ring. Compared with C-1 and C-2, the N-ε_h relation curve for C-0 is more representative. In particular, following the axial compression yield stage of the specimen, the hoop strain of the steel pipe increased rapidly, with the external steel tube restraining the core SLC significantly. By comparing Figs. 5(a) and 4(a), it can be shown that the growth rate of the hoop tensile strain was much greater than that of the axial compressive strain for circular specimen, and the hoop strain of the steel tube under the same load was also greater than the axial strain, showing that the external steel tube was subjected to hoop tension rather than axial compression at this point. Before the hoop strain gauge failed, the hoop strain in the C-0 steel tube was more than 12,000 $\mu\varepsilon$, meaning that the hoop tensile performance of material for the external circular steel tube had exhibited fully. Due to

Table 4 Comparison between measured results and calculated results for the ultimate bearing capacity for circular specimens

No.	N_u /kN	Unified strength theory				Limit equilibrium theory		Superposition theory					
		Zhong Shantong equation		Han Linhai equation		CECS 28:2012		AIJ-1997		EC4-2004		ACI-2005	
		N_c/kN	N_c/N_u	N_c/kN	N_c/N_u	N_c/kN	N_c/N_u	N_c/kN	N_c/N_u	N_c/kN	N_c/N_u	N_c/kN	N_c/N_u
C-0	1144	1276	1.115	1213	1.060	1647	1.440	982	0.858	780	0.682	663	0.580
C-1	1164	1535	1.319	1463	1.257	1846	1.586	1179	1.013	934	0.802	805	0.692
C-2	1078	1693	1.571	1615	1.498	1975	1.832	1293	1.199	1024	0.950	888	0.824
Average value			1.335		1.272		1.619		1.024		0.811		0.698
Standard deviation			0.186		0.179		0.162		0.139		0.110		0.100
Variation coefficient			0.139		0.141		0.100		0.136		0.135		0.143

Table 5 Comparison between measured results and calculated results for the ultimate bearing capacity for square specimens

No.	N_u/kN	Unified strength theory				Superposition theory							
		Zhong Shantong equation		Han Linhai equation		CECS159:2004		AIJ-1997		EC4-2004		ACI-2005	
		N_c/kN	N_c/N_u	N_c/kN	N_c/N_u	N_c/kN	N_c/N_u	N_c/kN	N_c/N_u	N_c/kN	N_c/N_u	N_c/kN	N_c/N_u
S-0	1201	1091	0.908	1090	0.828	994	0.828	866	0.721	823	0.685	0.908	0.527
S-1	1165	1397	1.199	1393	1.052	1226	1.052	1063	0.912	978	0.839	1.199	0.670
S-2	1013	1572	1.552	1564	1.343	1360	1.343	1177	1.162	1068	1.054	1.552	0.856
Average value			1.220		1.216		1.074		0.932		0.860		0.684
Standard deviation			0.263		0.260		0.211		0.180		0.151		0.135
Variation coefficient			0.216		0.214		0.196		0.194		0.176		0.197

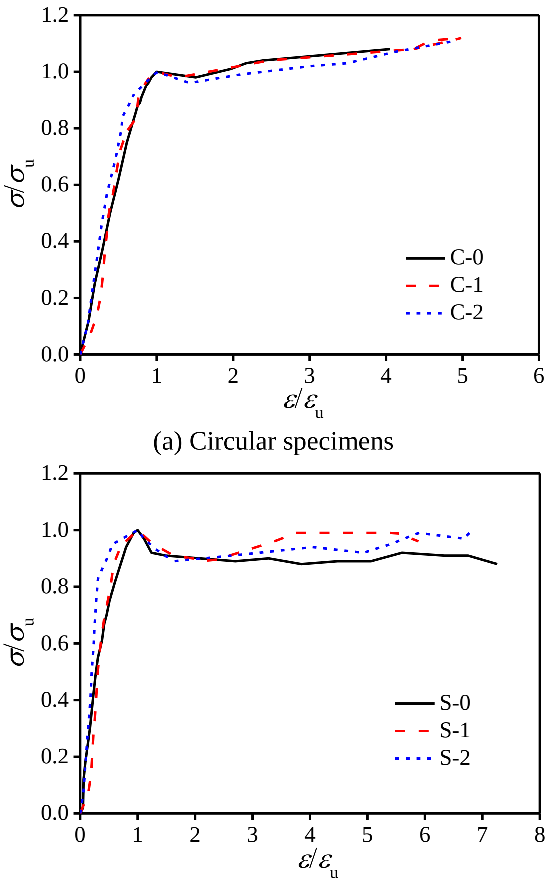

(a) Circular specimens

(b) Square specimens

Fig. 6 Measured non-dimensional strain-stress curves for specimens

the early failure of the steel tube strain gauges in the square specimen, the measured data for the hoop tension strain in the test is low. However, by comparing Figs. 5(a) and 5(b), it can be seen that under the same load, the hoop strain of the circular specimen was larger than that of the square specimen. This is because the external circular steel tube constraining the core SLC binding was strong and uniform, and the measured Poisson's ratio for the circular steel tube was less than that of the square steel, and the circular steel tube gets involved in working state of constraints earlier than the square steel tube.

4. Calculation of the ultimate bearing capacity

To date, many studies of the ultimate bearing capacity of concrete-filled steel tubular members have been carried out. In these, the theories put forward for the ultimate bearing capacity of stub columns under axial compression are mainly the unified strength theory, the limit equilibrium theory and the superposition theory. Unified strength theory involves the Zhong Shantong equation (Zhong 2003) and the Han Linhai equation (Han 2016), while limit equilibrium theory involves CECS 28:2012 (2012), and superposition theory includes CECS 159:2004 (2004), the Japanese code AIJ-1997 (1997), European Association Standard EC4-2004 (2004), and American Standard ACI-2005 (2005). In order to investigate whether the existing calculation method is applicable to SLCFST stub columns, based on the test data, the ultimate bearing capacity of the specimen under axial compression is calculated using the above equations, procedures and specifications, and the calculated value (N_c) is compared with the measured value (N_u), as shown in Tables 4 and 5.

As shown in Tables 4 and 5, for the C-SLCFST and S-SLCFST stub columns, the calculated value based on Zhong Shantong equation and the Han Linhai equation of the unified strength theory and CECS 28:2012 of the limit equilibrium theory is larger than the measured value, so the design of the ultimate bearing capacity of SLCFST stub columns under axial compression may be risky according to the above theory. Meanwhile, based on the superposition theory, the calculated values of EC-4 and ACI-2005 are markedly lower than the measured values, in other words, the calculated value of the ultimate bearing capacity of SLCFST stub columns under axial compression based on this theory may be conservative. For the C-SLCFST stub columns, the calculated values based on AIJ-1997 of the superposition theory are in good agreement with the measured values, and the standard deviation and the coefficient of variation are both small. The ratio between the calculated value and the measured value is less discrete, and it is therefore suggested that the calculation of the ultimate bearing capacity of the C-SLCFST stub columns under axial compression should use AIJ-1997. For the S-SLCFST stub columns, the calculated values based on the CECS 159:2004 and AIJ-1997 standards of superposition theory are in good agreement with the measured values, and the ratio between the two is not very discrete. It is therefore recommended that CECS 159:2004 or AIJ-1997 are used for the calculation of the ultimate bearing capacity of the S-SLCFST stub columns.

5. Analysis of full stress-strain curves

In order to eliminate the influence of the changing parameters, the measured stress and strain of SLCFST stub columns were divided by the peak stress and the peak strain, respectively, and non-dimension stress-strain curves are obtained as shown in Fig. 6.

Each dimensionless stress-strain curve of the circular specimens in Fig. 6(a) can be divided into three parts: a linear ascending section, a slowly ascending stage and a later development stage. The mathematical expressions are fitted by the least squares method, the result is shown in Eq. (2).

$$\begin{cases} y = ax, & x < x_A \\ y = b(x-1.0)^3 + 1.0, & x_A \le x \le 1 \\ y = c(x-1.4)^2 + d, & x > 1 \end{cases} \tag{2}$$

In the above equation, $x = \varepsilon/\varepsilon_u$, $y = \sigma/\sigma_u$, where the parameters ε_u and σ_u represent the peak strain and peak stress for the circular specimen; x_A is the ratio of the elastic proportionality limit strain to the peak strain, and it is recommended to use $x_A = 0.60$; the range of variation of the parameter a is 1.24 to 1.49, and it is recommended to use a = 1.40 and b = 2.50; and the changing range of parameter c is 0.01 to 0.07, and it is recommended to use c = 0.02, d = 1.00.

$$\begin{cases} \sigma = a\dfrac{f_{scy}}{\varepsilon_{scy}}\varepsilon, & 0 \le \varepsilon < 0.6\varepsilon_{scy} \\ \sigma = b\dfrac{f_{scy}}{\varepsilon_{scy}^3}(\varepsilon-\varepsilon_{scy})^3 + f_{scy}, & 0.6\varepsilon_{scy} \le \varepsilon < \varepsilon_{scy} \\ \sigma = c\dfrac{f_{scy}}{\varepsilon_{scy}^2}(\varepsilon-1.4\varepsilon_{scy})^2 + df_{scy}, & \varepsilon > \varepsilon_{scy} \end{cases} \tag{3}$$

$$f_{scy} = \eta\,(1.212 + B\xi + C\xi^2)\,f_c \tag{4}$$

$$\varepsilon_{scy} = 4\varphi\,[\,1300 + 14.39f_c + 1400 + 40\,(\,f_c - 20\,)\,]\xi^{0.99} \tag{5}$$

Based on an analysis of the working mechanism and the mechanical properties of the C-SLCFST stub columns, and considering the change in the parameter of natural river sand replacement ratio, equations for the full stress-strain process curve of the specimen can be derived, and these are given in Eqs. (3) to (5).

In the above equation, f_{scy} is the strength index of the C-SLCFST stub columns under axial compression; ε_{scy} is the strain corresponding to the strength index of the C-SLCFST stub columns under axial compression; η and φ are correction factors associated with the replacement ratio, where $\eta = 0.91 - 0.27r$ and $\varphi = 1.2 + 0.2r$; $B = 0.176f_y/215 + 0.974$; and $C = -0.104f_c/20 + 0.0309$.

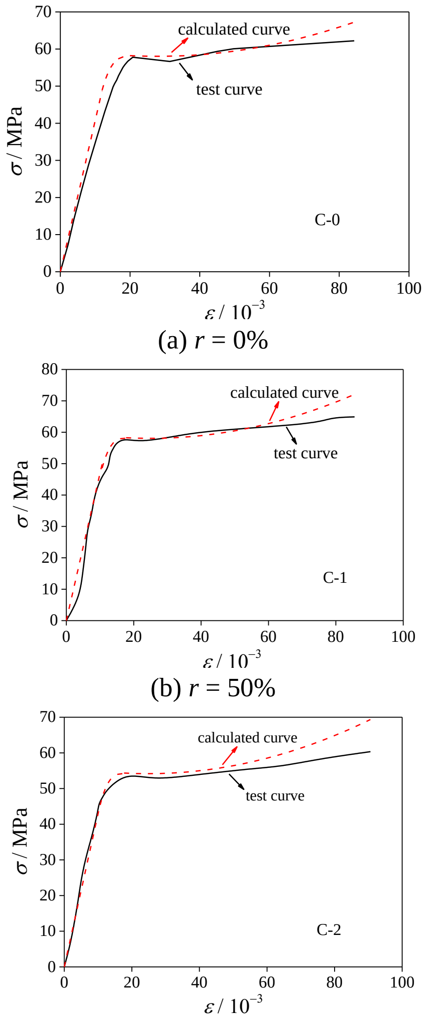

Fig. 7 Comparison between calculated curves and measured test curves for circular specimens

Each non-dimensional stress-strain curve of square specimens in Fig. 6(b) can be divided into four parts: a linear ascending section, a slowly ascending section, a descending section and a later development stage. The mathematical expression is fitted by the least squares method, the result is shown in Eq. (6)

$$\begin{cases} y' = ex', & x' < x_B \\ y' = (f-2)x'^3 + (3-2f)x'^2 + fx', & x' < 1 \\ y' = g(x'-1.7)^2 + 0.89, & 1 \le x' \le x_C \\ y' = 0.9, & x' > x_C \end{cases} \tag{6}$$

In the above equation, $x' = \varepsilon/\varepsilon'_u$ and $y' = \sigma/\sigma'_u$; ε'_u and σ'_u are the peak stress and peak strain of the square specimens, respectively; x_B is the ratio of the elastic ratio limit strain to the peak strain; x_C is the ratio of the limit strain to the peak strain in the descending section, and it is recommended to use $x_B = 0.5$; $x_C = 1.7$; the range of variation in the parameter

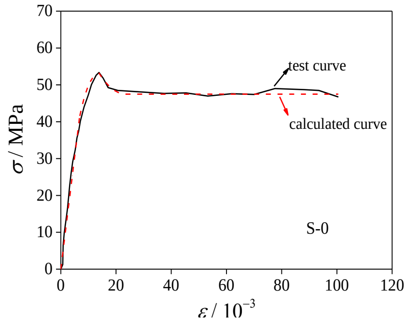

(a) r = 0%

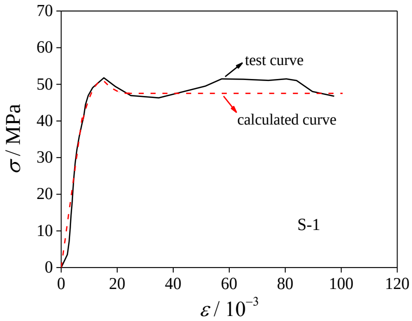

(b) r = 50%

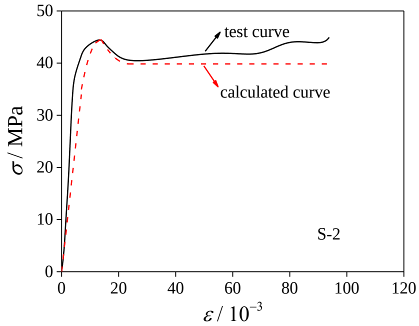

(c) r = 100%

Fig. 8 Comparison between calculated curves and measured test curves for square specimens

e is 1.49 to 2.28, and it is recommended to use e = 1.57; the range of variation in the parameter f is 1.78 to 3.33, and it is recommended to use f = 2.28; and g= 0.22.

By the similar way of C-SLCFST stub columns, the equations for the full stress-strain process curves of the S-SLCFST stub columns under axial compression are established by considering the variation of natural river sand replacement ratio, as shown in Eqs. (7) to (9).

$$\begin{cases} \sigma' = e\dfrac{f'_{scy}}{\varepsilon'_{scy}}\varepsilon', & 0 \le \varepsilon' < 0.5\varepsilon'_{scy} \\ \sigma' = \dfrac{f'_{scy}}{\varepsilon'^{3}_{scy}}[(f-2)\varepsilon'^{3} + (3-2f)\varepsilon'_{scy}\varepsilon'^{2} + f\varepsilon'^{2}_{scy}\varepsilon'], & 0.5\varepsilon'_{scy} \le \varepsilon' < \varepsilon'_{scy} \\ \sigma' = g\dfrac{f'_{scy}}{\varepsilon'^{2}_{scy}}(\varepsilon' - 1.7\varepsilon'_{scy})^{2} + 0.89f'_{scy}, & \varepsilon'_{scy} \le \varepsilon' \le 1.7\varepsilon'_{scy} \\ \sigma' = 0.9f'_{scy}, & \varepsilon' > 1.7\varepsilon'_{scy} \end{cases} \tag{7}$$

$$f'_{scy} = \eta' \,(\, 1.212 + B'\xi + C'\xi^{2}\,)\, f_c \tag{8}$$

$$\varepsilon'_{scy} = 4\varphi' \,[\, 1300 + 14.39 f_c + 1400 + 40\,(\, f_c - 20\,)\,]\, \xi^{0.99} \tag{9}$$

where f'_{scy} is the strength index of the S-SLCFST stub columns under axial compression; ε'_{scy} is the strain corresponding to the strength index of the S-SLCFST stub columns under axial compression; η' and φ' are correction factors associated with the replacement ratio, where η' = 1.10 − 0.48r and φ' = 1.60 − 0.92(r-0.70)^2; B' = 0.131f_y/235 + 0.723; and C' = −0.07f_c/20 + 0.026.

A comparison of the calculated stress-strain curves and tested stress-strain curves for the C-SLCFST and S-SLCFST stub columns are shown in Figs. 7 and 8. Obviously, it can be indicated that calculated stress-strain curves are in good agreement with tested stress-strain curves for circular specimens and square specimens. Thus, Eqs. (3) to (5) and (7) to (9) can be used to calculate the full stress-strain curves for the C-SLCFST and S-SLCFST stub columns manufactured in this study.

To be sure, for the validation of proposed models in Eqs. (3) and (7), another set of results from other references will be used in the further study.

6. Conclusions

Axial compression test and analysis of six SLCFST stub columns specimens are carried out in this study. The following conclusions are obtained:

• The peripheral steel tube of the SLCFST stub columns buckles outward, and the core SLC is crushed. The destructive positions of the circular specimen appear in the upper, lower and middle regions, while destructive positions of square specimens are mainly in the upper region; the destructive degree of square specimens is more serious than that of circular specimens, and some square specimens even appear the phenomenon that steel tube was tearing.

• The measured nominal stress-strain curves for all SLCFST stub columns have three distinct stages: a linear rise, a slow growth and a slow drop/steady development. In terms of force performance, there are three stages in the axial compression process of SLCFST stub columns: an elastic, an elastic-plastic and a plastic stage.

• In the early axial compression stage of C-SLCFST stub columns, the relationship between load and the axial or hoop strain shows a linear rise, when the curve of load-axial strain or load-hoop strain reach the turning point, there is a long plateau of plastic deformation. The axial compression and hoop tension performance of C-SLCFST stub columns have been fully developed.

• Based on the superposition theory, it is suggested that AIJ-1997 be used to calculate and design the ultimate bearing capacity for C-SLCFST stub columns. CECS 159:2004 or AIJ-1997 should be applied in the designing and calculation of the ultimate bearing capacity for S-SLCFST stub columns.

• Equations for the full stress-strain curves of the SLCFST stub columns are put forward with using the parameter of natural river sand replacement ratio, and the calculated curves show good agreement with the measured curves.

Acknowledgments

This work was financially supported by the Science and Technology Breakthrough Project of Henan Province (172102210285), the Fundamental Research Funds for the Universities of Henan Province (NSFRF170921), and the Safe Production Project of Key Technology for Major Accident Prevention and Control (Henan-0006-2016AQ).

References

Abdelgadir, E., Ji, B.H., Fu, Z.Q. and Hu, Z.Q. (2011), "The behaviour of lightweight aggregate concrete-filled steel tube columns under eccentric loading", *Steel Compos. Struct.*, **11**(6), 469-488.

ACI-2005 (2005), *Building Code Requirements for Structural Concrete and Commentary*, American Concrete Institute, Detroit, U.S.A.

AIJ-1997 (1997), *Recommendations for Design and Construction of Concrete-Filled Steel Tubular Structures*, Architectural Institute of Japan, Tokyo, Japan.

AL-Eliwi, B.J.M., Ekmekyapar, T., Faraj, R.H., Gogus, M.T. and AL-Shaar, A.A.M. (2017), "Performance of lightweight aggregate and self-compacted concrete-filled steel tube columns", *Steel Compos. Struct.*, **25**(3), 299-314.

Amel, C.L., Kadri, E.H., Sebaibi, Y. and Soualhi, H. (2017), "Dune sand and pumice impact on mechanical and thermal lightweight concrete properties", *Constr. Build. Mater.*, **133**, 209-218.

Assi, I.M., Qudeimat, E.M. and Hunaiti, Y.M. (2003), "Ultimate moment capacity of foamed and lightweight aggregate concrete-filled steel tubes", *Steel Compos. Struct.*, **3**(3), 199-212.

Ayati, B., Ferrándiz-Mas, V., Newport, D. and Cheeseman, C. (2018), "Use of clay in the manufacture of lightweight aggregate", *Constr. Build. Mater.*, **162**, 124-131.

Carrillo, J., Lizarazo, J.M. and Bonett, R. (2015), "Effect of lightweight and low-strength concrete on seismic performance of thin lightly-reinforced shear walls", *Eng. Struct.*, **93**, 61-69.

CECS 159 (2004), *Technical Specification for Structures with Concrete-Filled Rectangular Steel Tube Members*, China Planning Press, Beijing, China.

CECS 28 (2012), *Technical Specification for Concrete-Filled Steel Tubular Structure*s, China Planning Press, Beijing, China.

Chien, L.K., Kuo, Y.H., Huang, C.H., Chen, H.J. and Cheng, P.H. (2014), "Flexural behaviour of reinforced lightweight concrete beams under reversed cyclic loading", *Struct. Eng. Mech.*, **52**(3), 559-572.

Choi, S.J., Yang, K.H., Sim, J.I. and Choi, B.J. (2014), "Direct tensile strength of lightweight concrete with different specimen depths and aggregate sizes", *Constr. Build. Mater.*, **63**, 132-141.

Dong, W., Shen, X.D., Xue, H.J., He, J. and Liu, Y. (2016), "Research on the freeze-thaw cyclic test and damage model of Aeolian sand lightweight aggregate concrete", *Constr. Build. Mater.*, **123**, 792-799.

EC4-2004 (2004), *Design of Composite Steel and Concrete Structure*s, European Committee for Standardisation, Brussels, Belgium.

Fu, Z.Q., Ji, B.H., Ge, H.B. and Yang, M. (2016), "Combined strength of lightweight aggregate concrete-filled steel tube", *Mater. Res. Innov.*, **19**(5), 898-901.

Fu, Z.Q., Ji, B.H., Maeno, H., Eizien, A. and Chen, J. (2014), "Flexural behavior of lightweight aggregate concrete-filled steel tube", *Adv. Steel Constr.*, **10**(4), 385-403.

Ghannam, S., Jawad, Y.A. and Hunaiti, Y. (2004), "Failure of lightweight aggregate concrete-filled steel tubular columns", *Steel Compos. Struct.*, **4**(1), 1-8.

Han, L.H. (2016), *Concrete-Filled Steel Tubular Structures, Theory and Practice*, 3rd Edition, Science Press, Beijing, China.

Liu, F., Gardner, L. and Yang, H. (2014), "Post-fire behaviour of reinforced concrete stub columns confined by circular steel tubes", *J. Constr. Steel Res.*, **102**(11), 82-103.

Meng, W. and Khayat, K. (2017), "Effects of saturated lightweight sand content on key characteristics of ultra-high-performance concrete", *Cement Concrete Res.*, **101**, 46-54.

Min, Y.U., Zha, X., Ye, J.Q. and Li, Y.T. (2013), "A unified formulation for circle and polygon concrete-filled steel tube columns under axial compression", *Eng. Struct.*, **49**(2), 1-10.

Montejo, L.A. (2012), "Seismic performance evaluation of reinforced concrete-filled steel tube pile/column bridge bents", *J. Earthq. Eng.*, **16**(3), 401-424.

Obaidat, Y.T. and Haddad, R.H. (2016), "Prediction of residual mechanical behavior of heat-exposed LWAC short column: A NLFE model", *Struct. Eng. Mech.*, **57**(2), 265-280.

Shafigh, P., Alengaram, U.J., Mahmud, H.B. and Jumaat, M.Z. (2013), "Engineering properties of oil palm shell lightweight concrete containing fly ash", *Mater. Des.*, **49**(1), 613-621.

Tang, C.W. (2017), "Uniaxial bond stress-slip behaviour of reinforcing bars embedded in lightweight aggregate concrete", *Struct. Eng. Mech.*, **62**(5), 651-661.

Tao, Z., Han, L.H., Uy, B. and Chen, X. (2016), "Post-fire bond between the steel tube and concrete in concrete-filled steel tubular columns", *J. Constr. Steel Res.*, **67**(3), 484-496.

Tu, Y.Q., Shen, Y.F., Zeng, Y.G. and Ma, L.Y. (2014), "Hysteretic behaviour of multi-cell T-shaped concrete-filled steel tubular columns", *Thin Wall Struct.*, **85**, 106-116.

Yang, K.H. and Ashour, A.F. (2011), "Aggregate interlock in lightweight concrete continuous deep beams", *Eng. Struct.*, **26**(1), 136-145.

Zhang, D.J., Ma, Y.S. and Wang, Y. (2015), "Compressive behaviour of concrete filled steel tubular columns subjected to long-term loading", *Thin Wall Struct.*, **89**, 205-211.

Zhang, X.G., Deng, D.P. and Yang, J.H. (2018), "Mechanical properties and conversion relations of strength indexes for stone/sand-lightweight aggregate concrete", *Adv. Mater. Sci. Eng.*, 5402953.

Zhang, X.G., Kuang, X.M., Yang, J.H. and Wang, S.R. (2017), "Experimental study on mechanical properties of lightweight concrete with shale aggregate replaced partially by nature sand", *Electron. J. Struct. Eng.*, **17**(1), 85-94.

Zhong, S.T. (2003), *The Concrete-Filled Steel Tube Structures*, Tsinghua University Press, Beijing, China.

CC